



AIAA 2000-0896

Simulation of the Dynamics of Micro Air Vehicles

Ravi Ramamurti and William Sandberg

Laboratory for Computational Physics and Fluid Dynamics
Naval Research Laboratory
Washington, D.C. 20375

Rainald Löhner

Institute for Computational Sciences and Informatics
The George Mason University
Fairfax, VA 22030

**38th Aerospace Sciences
Meeting & Exhibit
10-13 January 2000 / Reno, NV**

Simulation of the Dynamics of Micro Air Vehicles

Ravi Ramamurti, William Sandberg and Rainald Löhner*

Laboratory for Computational Physics and Fluid Dynamics
Naval Research Laboratory, Washington, D.C. 20375

*Institute for Computational Sciences and Informatics
The George Mason University, Fairfax, VA 22030

ABSTRACT

A finite element flow solver based on unstructured grids is employed for studying the aerodynamic characteristics of Micro Air Vehicles. Inviscid and viscous flow simulations were performed for two different Micro Air Vehicles developed at NRL. Lift and drag force variations were computed for a range of flow angles and control surface angles. The Baldwin-Lomax turbulence model was employed for turbulent flows. An actuator disk model was used to study the effect of the propeller flow.

INTRODUCTION

Unmanned aerial vehicles (UAVs) play an important role in reconnaissance and war fighting [1-5]. Recently, micro air vehicles (MAVs) [6] have been of significant interest to the war fighting as well as the intelligence collection communities. MAVs have the potential for providing a new technological capability that can be used not only by the military, but also in commercial applications including law enforcement, environmental hazard detection and assessments, and inspection of the interior of large buildings. There is more to designing micro air vehicles than just scaling down the dimensions of UAVs. The aerodynamics of the MAVs in the low Reynolds number (Re) regime differs significantly from the aerodynamics of mini vehicles, such as the UAVs. The objective of the computations discussed in this paper is to investigate the inviscid and low-Re aerodynamics of novel MAV designs.

In this study, a finite element based incompressible flow solver is employed. The simple elements enable the flow solver to be as fast as possible, reducing the overhead in building element matrices, residual vectors etc. The governing equations are written in Arbitrary Lagrangian Eulerian form, which enables simulation of flow with moving bodies. For viscous flow cases, the mesh requirement for resolving the boundary layer is met by employing arbitrary semi-structured grids close to wetted surfaces and wakes. An actuator disk model is employed for modeling the propeller flow. Turbulent flow simulations are performed using the Baldwin-Lomax turbulence model. The details of the flow solver, the rigid body motion and adaptive remeshing

are given by Ramamurti *et al.* [7] and are summarized next.

THE INCOMPRESSIBLE FLOW SOLVER

The governing equations employed are the incompressible Navier-Stokes equations in Arbitrary Lagrangian Eulerian (ALE) formulation which are written as

$$\frac{\mathbf{v}}{t} + \mathbf{v} \cdot \nabla_a \mathbf{v} + \nabla_a p = \mathbf{f}, \quad (1)$$

$$\nabla_a \cdot \mathbf{v} = 0, \quad (2)$$

where p denotes the pressure, $\mathbf{v}_a = \mathbf{v} - \mathbf{w}$ the advective velocity vector (flow velocity \mathbf{v} minus mesh velocity \mathbf{w}) and both the pressure p and the stress tensor $\boldsymbol{\tau}$ have been normalized by the (constant) density ρ , are discretized in time using an implicit time stepping procedure. It is important for the flow solver to be able to capture the unsteadiness of a flow field, if such exists. The present flow solver is time-accurate, allowing local timestepping as an option. The resulting expressions are subsequently discretized in space using a Galerkin procedure with linear tetrahedral elements. In order to be as fast as possible, the overhead in building element matrices, residual vectors, etc. should be kept to a minimum. This requirement is met by employing simple, low-order elements that have all the variables (u, v, w and p) at the same node location. The resulting matrix systems are solved iteratively using a preconditioned gradient algorithm (PCG). The preconditioning is achieved through linelets as described by Martin and Löhner [8]. The flow solver has been successfully evaluated for both 2-D and 3-D,

This paper is a work of the U.S. Government and is not subject to copyright protection in the United States.

laminar and turbulent flow problems by Ramamurti *et al.* [9,10].

DESCRIPTION OF THE MICRO AIR VEHICLE MODEL

The design of the basic MAV model examined in this study was developed at the Naval Research Laboratory, and is called the Micro Tactical Expendable (MITE). The wingspan of the vehicle is 6" with a span to wing chord aspect ratio of 1.25. It is driven by a single engine with two counter-rotating propellers. The main airfoil is a NACA 0006 section and the end plates are NACA0015 sections. The control surface for the configuration is a wedge airfoil

which combines the functions of a rudder and an aileron. A schematic of the configuration is shown in Fig. 1. The NRL MAV was recently highlighted in a special MAV report [11].

Another MAV configuration that was tested is called the MITE2. This is a larger model with a 14.5" wingspan and a chord of 10". This configuration was successfully flown at NRL. This configuration differs from the MITE in that it has two tail fins acting as roll stabilizers and elevons, which combine the functions of the elevators and ailerons, as the primary control surface, and is shown in Fig. 2.

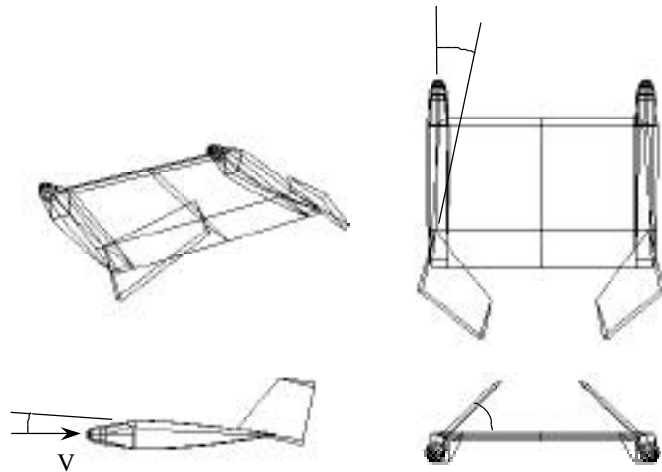


Fig. 1. Schematic of MITE showing the control surface angles

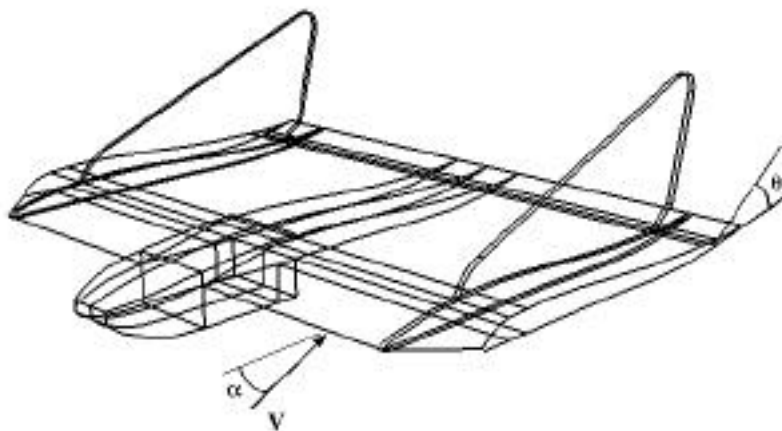


Fig. 2. Schematic of the MITE2 configuration

DISCUSSION OF RESULTS

MITE

Three-dimensional flow past the MITE was computed at various angles of attack, α , ranging from 0° to 14.5° , of the main foil. These results were obtained using inviscid calculations on a grid consisting of approximately 160K points and 860K tetrahedra. Computations were performed over half the vehicle assuming symmetry about the $z=0$ plane. The length scale was non-dimensionalized with the chord length and the inflow velocity with the free stream velocity. The aerodynamic characteristics of the vehicle were also evaluated for several cant angles β (see Fig. 1) and are shown in Fig. 3. In this figure, L and D are the non-dimensional lift and drag forces, respectively, computed by integrating the surface pressure distribution over half the vehicle. The lift force L increases linearly with α , as expected. The calculations show that the lift to drag ratio (L/D) attains a maximum around $\alpha = 4.5^\circ$, for the range of values of β from 30° to 45° . The results show that L/D increases as β is decreased from 45° to 30° . This is due to the increase in lift at $\alpha = 30^\circ$. The drag is almost the same for all the cant angles tested. The surface pressure distribution on the configuration and on the symmetry plane, for $\alpha = 45^\circ$ and $\beta = 0^\circ$ is shown in Fig. 4. It can be seen that the maximum pressure is at the stagnation regions at the nose of the end plate and at the leading edge of the main airfoil, and the minimum value occurs at the junction of the main airfoil and the control surface. The convergence history for the case of $\alpha = 0^\circ$, is shown in Fig. 5. The grid that was employed for this case consisted of 157K points, 856K tetrahedral elements. It can be seen that the residual in pressure

dropped by more than 3 orders of magnitude in 500 iterations.

Laminar and turbulent flow were computed past this configuration for a Reynolds number (Re), based on the chord of the main airfoil. The Baldwin-Lomax model [12] was employed to model the eddy viscosity. The contribution of the pressure and the viscous forces to the lift and drag are shown in Table 1. The L/D for the laminar case, at $Re = 50,000$, is reduced from the inviscid result of 7.3 to 1.46, primarily due to the viscous drag.

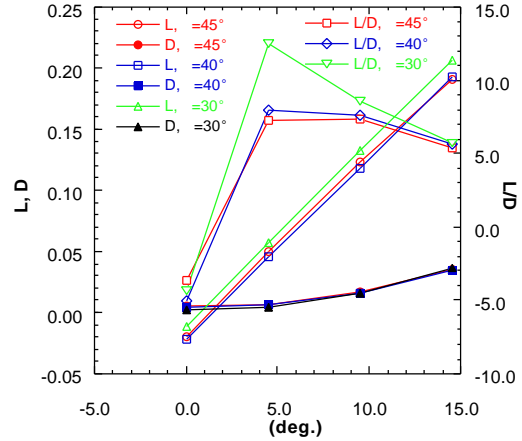


Fig. 3. Aerodynamic Characteristics of MITE

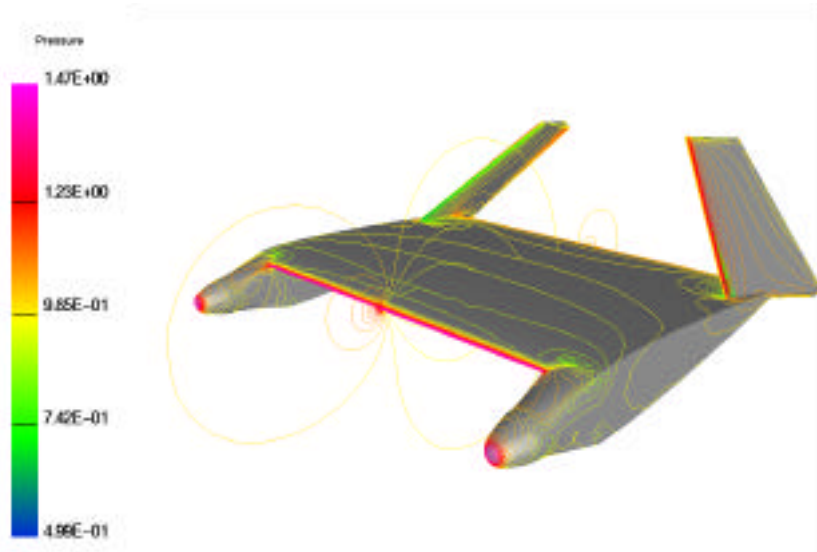


Fig. 4. Surface Pressure Distribution on MITE at $\alpha = 45^\circ$ and $\beta = 0^\circ$.

Re	Drag(pr.)	Drag(visc.)	Total Drag	Lift (pr.)	Lift (visc.)	Total Lift	L/D
Euler	6.80e-03	0.00e+00	6.80e-03	4.97e-02	0.00e+00	4.97e-02	7.31
50000 laminar	9.24e-03	1.45e-02	2.37e-02	3.52e-02	-4.45e-04	3.48e-02	1.46
100000 laminar	7.97e-03	5.21e-03	1.32e-02	4.05e-02	-1.22e-04	4.04e-02	3.06
100000 turbulent	9.14e-03	8.24e-03	1.74e-02	3.31e-02	-2.64e-04	3.29e-02	1.89

Table 1. Variation of Lift and Drag for the MITE

As Re is increased further, the L/D ratio increases to 3.06, due to the increase in lift and a slight drop in the drag force. For the turbulent case, the entire model was assumed to be in a fully turbulent flow. The drag due to the pressure and the viscous components increases by a modest amount, compared to the laminar case. The lift force is also slightly reduced, resulting in a decrease of L/D, to a value of 1.89. The convergence history for the laminar case is shown in. Again, the pressure converges by more than 3 orders of magnitude in 700 iterations.

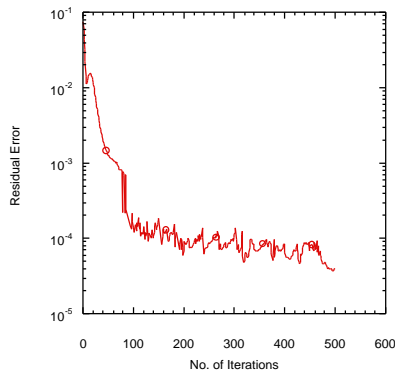


Fig. 5. Convergence history for laminar flow

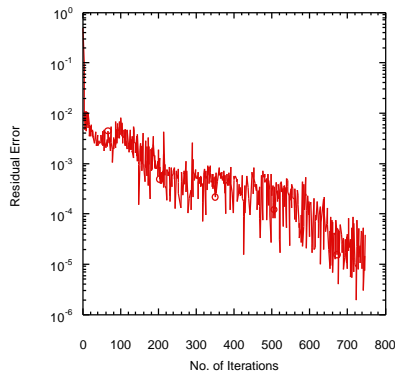


Fig. 6. Convergence history for laminar flow

Effect of Fuselage

The initial MITE configuration shown in Fig. 1 was modified to include a fuselage at the center with the entire fuselage located below the leading edge of the main airfoil, and the control surface cant angle at $\alpha = 45^\circ$. The grid that was employed for this configuration consisted approximately 187K points and 1.03M tetrahedral elements. The third configuration that was evaluated was the MITE configuration with the fuselage smoothly joined on the upper surface of the main airfoil. A grid with 211K points and 1.16M tetrahedral elements was employed for this case. The effect of the fuselage on the L/D characteristic of the vehicle was also studied at selected angles of attack and the results are plotted in Fig. 7. The addition of the fuselage lowers the lift and the L/D ratio at $\alpha = 4.5^\circ$. The maximum L/D ratio, occurs at an angle of attack $\alpha = 9.5^\circ$. The drag for all the three configurations considered are nearly the same. The surface pressure distribution for configuration 3 is shown in Fig. 8.

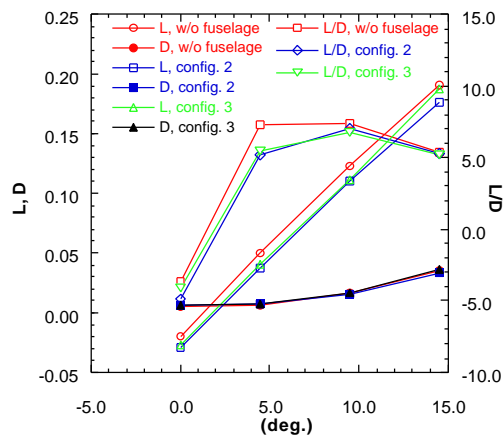


Fig. 7. Effect of fuselage on the lift and drag

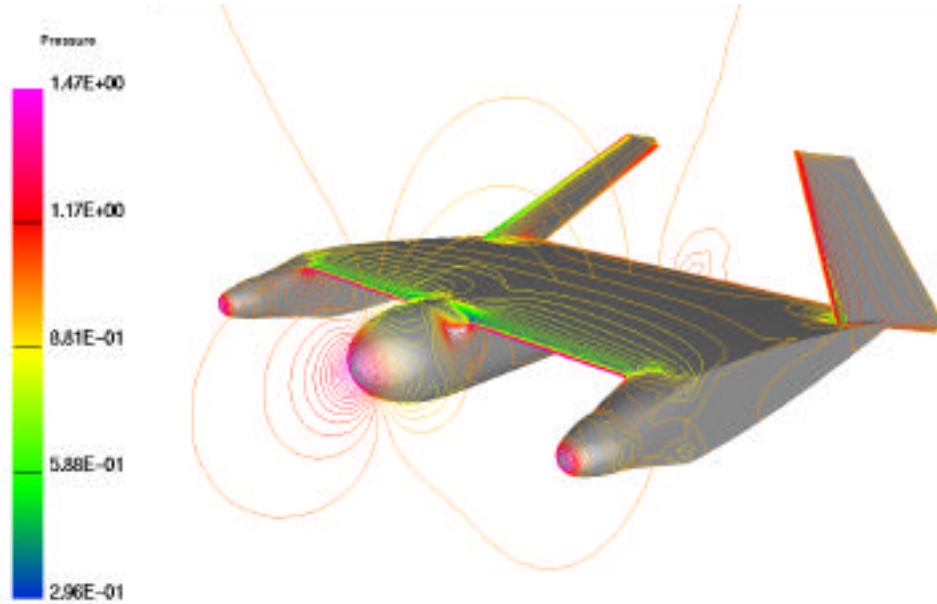


Fig. 8. Surface pressure distribution over the MITE configuration with fuselage, $\alpha = 45^\circ$ and $\beta = 0^\circ$

Effect of Propeller

In order to study the effect of the flow due to the propeller, we could employ the adaptive remeshing flow solver to simulate the flow past the moving blades and the interaction of this flow with the vehicle. This computation would be long due to the unsteady nature, and computationally expensive due to the remeshing around moving bodies. The objective of this study is to evaluate several configurations at various flow angles and control surface orientations. Hence, a simpler model to mimic the flow due to the propeller, such as an actuator disk model is employed.

The region where the propeller is situated, shown in Fig. 9, is marked. In this region, source terms are added as body forces in the momentum equation, Eq. 1. This model has been successfully employed by Oh *et al* [13] for modeling the flow in a ducted propulsor. The source strength for the propeller region is determined from the thrust per unit volume. First, a constant body force term in the x -direction is added. The strength of the source was computed to compensate the drag force. The lift force increased from 0.038 to 0.039, but the drag force also increases from a value of 0.007 to 0.010. Hence, the source strength was increased by an order of magnitude. For this case, although the lift increased to 0.045, the drag also increased to 0.015, reducing the L/D to approximately 3.06. Hence, a momentum source which has the effects of a rotating propeller with appropriate distribution in the radial direction, is desired. The effect of radial variation of the source will be reported in a later work.

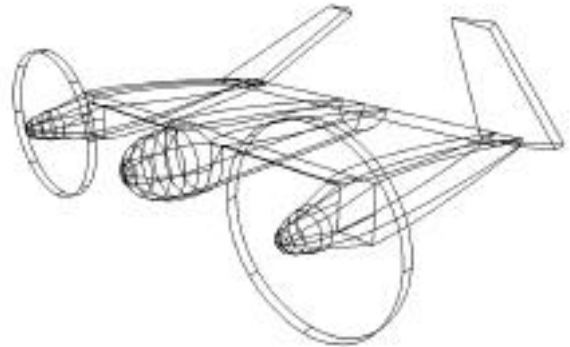


Fig. 9. MITE configuration with the propeller

MITE2 Configuration

The elevon deflection angle δ , of the MITE2 configuration, shown in Fig. 2, was varied in the range from -15° to $+15^\circ$; positive angles are for the elevon deflected in the counter-clockwise direction from the original position. The variation of the coefficient of lift with change in angle of attack for various elevon angle is shown in Fig. 10. The lift coefficient is obtained by non-dimensionalizing the lift force with the dynamic head and the area and is given by

$$C_L = \frac{F_L}{\frac{1}{2} \rho V^2 L_{ref}^2}, \quad C_D = \frac{F_D}{\frac{1}{2} \rho V^2 L_{ref}^2} \quad (3a-c)$$

$$\text{and } C_{Mx} = \frac{M_x}{\frac{1}{2} \rho V^2 L_{ref}^3}$$

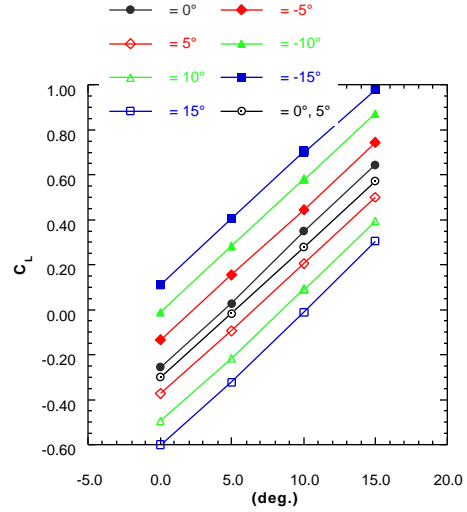
Here, F_L and F_D are the lift and drag forces, M_x is the moment about x -axis, V is the inflow velocity, and L_{ref} is the reference length. The L_{ref} is taken to be 10" for this configuration. It is clear from Fig. 10a, that C_L varies linearly with α for all the elevon angles tested, and $dC_L/d\alpha$ is approximately 3.43/radian. For the MITE configuration, with L_{ref} being unity, at an angle of attack $\alpha = 14.5^\circ$, and $\delta = 30^\circ$, the lift force is approximately 0.21, resulting in a C_L of 0.41. For the MITE2 configuration, the C_L exceeds this value for all elevon angles $\delta = 5^\circ$. The cases where the two elevons of the vehicle are deflected asymmetrically are denoted by two values for the angle δ . In Fig. 10a, the variation of lift for a differential deflection of 5° , falls between the curve corresponding to the case where both the elevons are deflected by 0° and 5° . The variation of the lift coefficient with angle of attack when the elevons are deflected asymmetrically is shown in Fig. 10b. For all the deflections studied, the $dC_L/d\alpha$ is almost constant, except for the case when one of the elevon is deflected by $+15^\circ$. In this case, the pressure on the lower side of the elevon is reduced resulting in a loss of lift at high angles of attack.

The variation of C_L with respect to elevon angle is shown in Fig. 11. It is clear that the variation is almost linear with $dC_L/d\delta$ of approximately 1.36/radian.

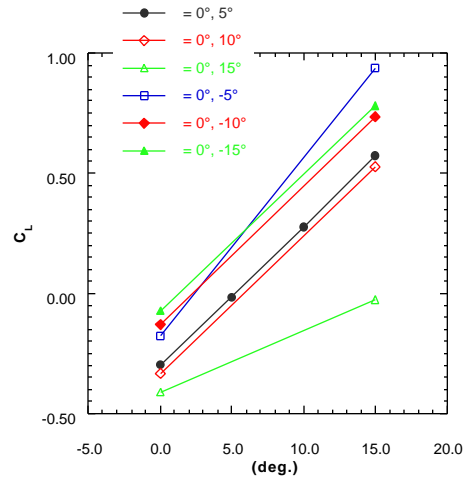
The variation of the drag coefficient is shown in Fig. 12. For all the cases where the elevons are deflected by a positive angle, the drag coefficient is a minimum at $\alpha = 5^\circ$, and increases with further increase in α . For the negative deflection cases the minima occurs at 0° , and increases with increase in α . The drag coefficient for the case of the split elevon, falls between the values corresponding to $\delta = 0^\circ$ and 5° .

The variation of the ratio of C_L/C_D is shown in Fig. 13. At $\alpha = 0^\circ$, the C_L/C_D is negative except for $\delta = -15^\circ$. For all the cases with negative elevon deflection, the C_L/C_D achieves a maximum at $\alpha = 5^\circ$; for positive deflection angles, there is a drop in C_L/C_D when the α is increased to 5° , and recovers with further increase in α . It is interesting to note that at $\alpha = 15^\circ$, all the cases come together to a value of around 5.0, perhaps due to the dominance of the wing-fuselage flow at high angles of attack.

The variation of the roll moment is shown in Fig. 14. It can be seen that for both angles of attack tested, the roll moment varies linearly with elevon deflection angle. The $dC_{Mx}/d\delta$ is approximately 0.16/radian.



a. symmetric deflection of elevons



b. asymmetric deflections of elevons

Fig. 10. Variation of lift coefficient with angle of attack for various elevon angles

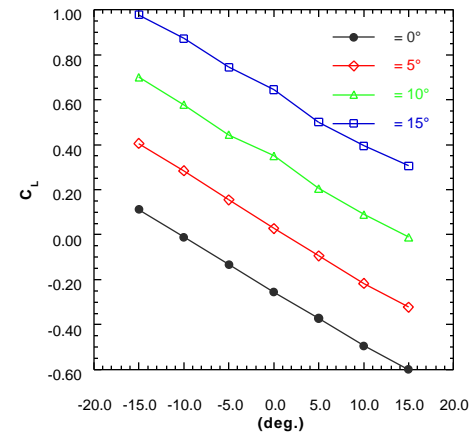


Fig. 11. Variation of lift coefficient with elevon angle

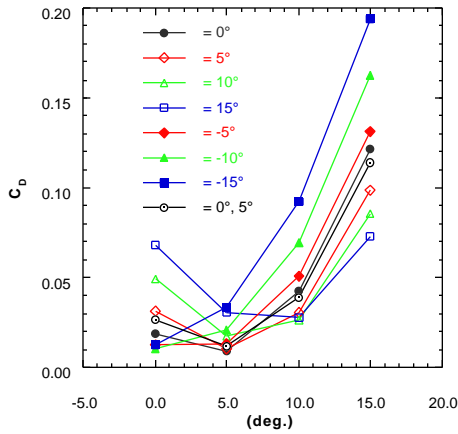


Fig. 12. Variation of drag coefficient with angle of attack, MITE2 configuration

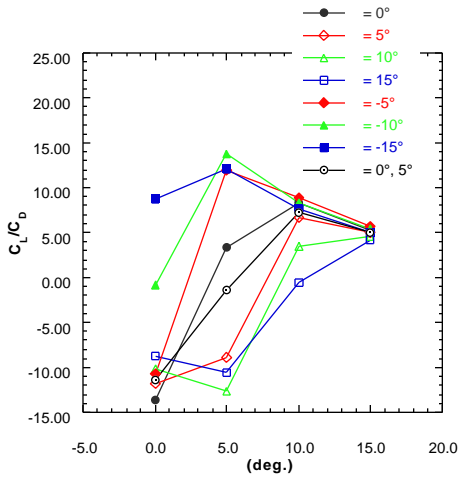


Fig. 13. Variation of C_L/C_D with angle of attack

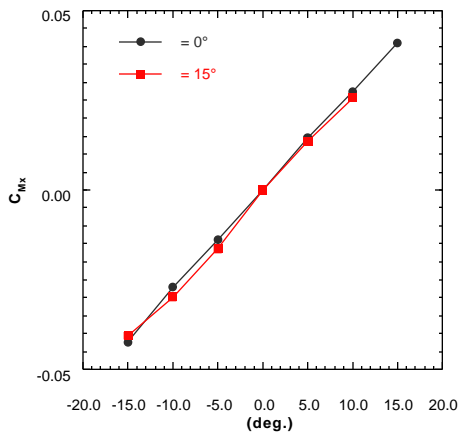
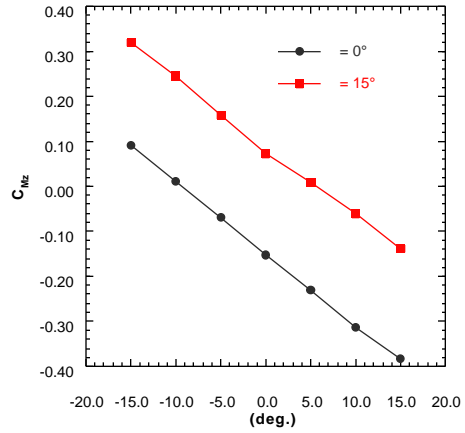
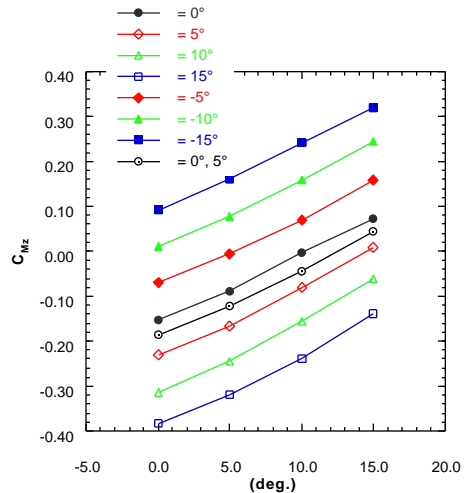


Fig. 14. Variation of roll moment with elevon angle

The variation of the pitch moment about the center of gravity of the vehicle is shown in Fig. 15. From Fig. 15a, it can be seen that the pitch moment varies linearly with α , and the slope is approximately 0.91/radian. The variation with the angle of attack is shown in Fig. 15b. As α is increased, the C_{M_z} increases for all elevon angles.



a. Effect of elevon angle



b. Effect of angle of attack

Fig. 15. Variation of coefficient of pitch moment

SUMMARY AND CONCLUSIONS

A finite element flow solver based on unstructured grids has been employed to study the aerodynamic characteristics of micro air vehicles. Several configurations developed at NRL, the MITE, with and without the fuselage, and the MITE2 were evaluated. Both laminar and turbulent flows past these configurations were computed for selected cases. For the MITE configuration without the fuselage, the L/D

ratio attains a maximum value of 12.5 for a control surface cant angle = 30°, and at an angle of attack = 4.5°. The addition of fuselage lowers the L/D ratio at = 4.5°. For the MITE2 configuration, several computations were performed varying the angle of attack and the elevon angle. From these results, the characteristic derivatives were computed. These derivatives will serve as an input for a trajectory simulation. An actuator disk model was employed to simulate the effect of the propellers. A constant source distribution was used to test the correctness of the model. A more appropriate source distribution based on the blade geometry and load distribution will be employed in future work. For miniature air vehicles, the propeller is not an efficient mechanism for propulsion. For these vehicles, flapping foil propulsion is an attractive alternative. The lift and thrust enhancement in this mode of propulsion was studied in 2-D by Ramamurti *et. al* [14], and is being extended to three dimensions.

ACKNOWLEDGEMENTS

This work was supported by the Office of Naval Research through the Tactical Electronic Warfare Division of the Naval Research Laboratory. The authors would like to thank Mr. Kevin Ailinger for his assistance and support throughout the course of this work. This work was supported in part by a grant of HPC time from the DoD HPC Centers, ARL MSRC SGI-O2K and NRL SGI-O2K.

REFERENCES

1. Cook, N., "USA's revolutionary plan for air vehicles unveiled," *Jane's Defence Weekly*, March 1997.
2. Evers, S., " 'Culture of Innovation' return to UAV projects," *Jane's Defence Weekly*, March 1997.
3. Hewish, M, "Building a bird's-eye view of the battlefield," *Jane's International Defense Review*, February 1997.
4. Canan, J.W., "Seeing more, and risking less, with UAVs," *Aerospace America*, October 1999.
5. Wilson, R., "Mini Technologies for major impact," *Aerospace America*, May 1998.
6. Hewish, M., "Rucksack reece takes wing," *Jane's International Defense Review*, February 1997.
7. Ramamurti, R., Sandberg, W.C. and Löhner, R., "Simulation of a Torpedo Launch Using a 3-D Incompressible Finite Element Flow Solver and

Adaptive Remeshing," *AIAA Paper No. 95-0086*, January 1995.

8. Martin, D. and Löhner, R., "An Implicit Linelet-Based Solver for Incompressible Flows," *AIAA Paper No. 92-0668*, 1992.
9. Ramamurti, R. and Löhner, R., "Evaluation of an Incompressible Flow Solver Based on Simple Elements," *Advances in Finite Element Analysis in Fluid Dynamics*, 1992, FED Vol. 137, Editors: M.N Dhaubhadel et al., ASME Publication, New York, pp. 33-42.
10. Ramamurti, R., Löhner, R. and Sandberg, W.C., "Evaluation of Scalable 3-D Incompressible Finite Element Solver," *AIAA Paper No. 94-0756*, 1994.
11. Hewish, M., "A bird in hand, Miniature and micro air vehicles challenge conventional thinking," *Jane's International Defense Review*, November 1999.
12. Baldwin, B.S. and Lomax, H., "Thin Layer Approximation and Algebraic Model for Separated Turbulent Flows," *AIAA-78-257*, Washington, D.C., 1978.
13. Oh, C.K., Löhner, R., Ramamurti, R. and Sandberg, W.C., "An Actuator Disc Simulation of Body-Ducted Propulsor Flow," *APS Fluid Meeting*, New Orleans, LA , November 21-23, 1999.
14. Ramamurti, R., Sandberg, W.C. and Löhner, R., "Simulation of Flow about Flapping Foils Using a Finite Element Incompressible Flow Solver," *AIAA-99-0652*, Washington, D.C, 1999; in review *AIAA Journal*, 1999.